Earth, Planets and Space

TECHNICAL REPORT

Open Access

Estimation of paleo-permeability around a seismogenic fault based on permeability tensor from observable geometric information of quartz veins

Hinako Hosono[1,2], Takato Takemura[1*], Daisuke Asahina[2] and Makoto Otsubo[2]

Abstract

The mineral veins formed by filling tensile cracks record the accumulation of past hydraulic activities such as fluid migration in the damage zones of a fault. The purpose of this study is to estimate the fluid flow behavior around thrust faults using a three-dimensional permeability tensor from the geometric information of mineral veins. Here, the estimated permeability represents paleo-permeability when the mineral veins were open fractures. We attempted to estimate paleo-permeability in the damage zone around the Nobeoka Thrust fault by applying Oda's permeability tensor theory, as determined from the geometric information of mineral veins observed in the outcrop. In addition, in situ data acquisition and analytic techniques were developed to estimate a three-dimensional paleo-permeability tensor, and we estimated the paleo-permeability around the Nobeoka Thrust. As a result, the paleo-permeability tensor could be estimated from the geometric information of the mineral veins in the outcrop, which helped clarify the migration of fluids around the fault. Our results show that the paleo-permeability anisotropy and paleo-permeability value changed with distance from the fault core on the footwall; in particular, the maximum paleo-permeability increased from the damage zone to the fault core. In addition, the direction of maximum paleo-permeability shows that the fluid in the footwall migrated toward the fault plane or to the hanging wall immediately after the earthquake.

Keywords: Paleo-permeability, Earthquake, Subduction zone, Quartz vein

*Correspondence: takemura.takato@nihon-u.ac.jp

[1] Geomechanics Lab., Graduate School of Integrated Basic Sciences, Nihon University, Sakurajyosui 3-25-40, Setagaya, Tokyo 156-8550, Japan
Full list of author information is available at the end of the article

Graphical Abstract

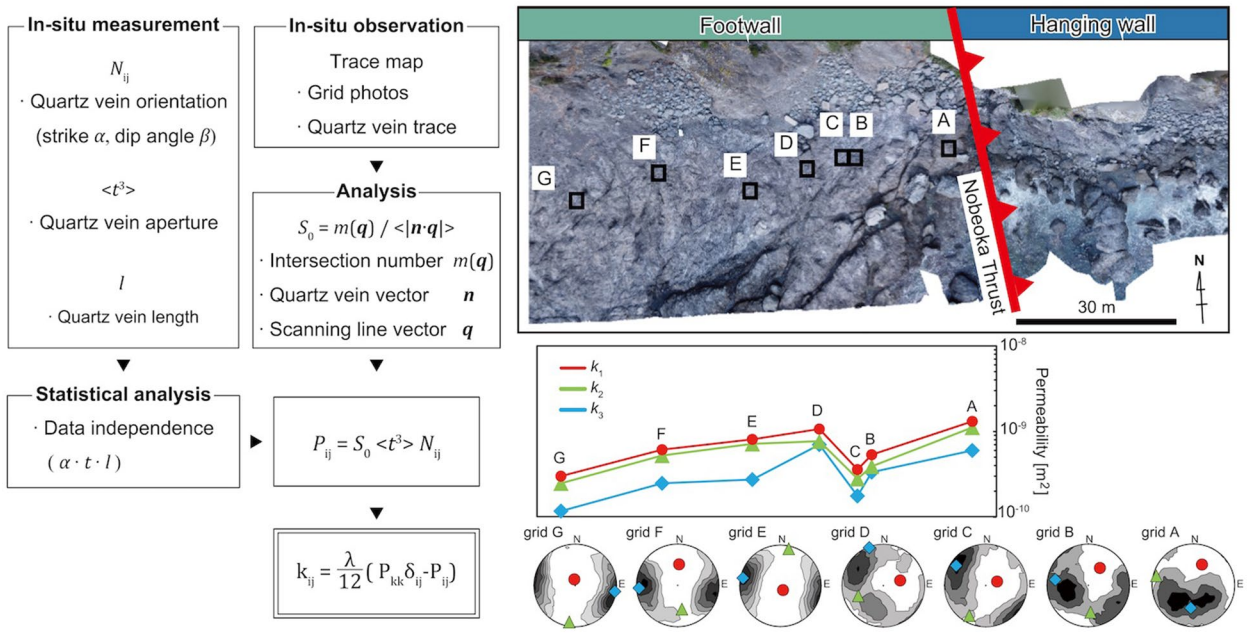

Introduction

Quantitative estimation of fluid flow behavior is key to understanding the mechanism of subduction zone earthquakes. It is well known that the decrease in effective stress, associated with increased fluid pressure, induces a decrease in the shear resistance of the fault plane in the preliminary stages leading to earthquakes (e.g., Hubbert and Rubey 1959; Sibson 2020). Recent observational advances have highlighted that high pore pressure regions are often present in the seismogenic regions of thrust fault zones (Bangs 1990; Park et al. 2010; Kamei et al. 2012; Tsuji et al. 2014). In the post-earthquake stage, fractures developed by fault movements accelerate the release of accumulated pore fluid, thereby reducing fluid pressure (Sibson 1990). This stage is encapsulated in the fault-valve model which explains the relationship between fluid pressure and slip strength on the fault plane (Sibson 1981, 1992). Furthermore, Sibson (1992) suggested that fracture self-sealing by hydrothermal precipitation is another factor that promotes an increase in the fluid pressure and slip strength of the fault plane. This implies that both pore pressure and sealing via mineral precipitates are important factors in the earthquake cycle. The importance of these two factors lies in the fact that the fluids migrating into the surrounding pores and fractures cause chemical reactions that alter the mechanical and hydraulic properties of the fault zone (Scholz 2019). Therefore, permeability estimates can provide a better understanding of fluid accumulation and discharge during fault-valve behavior. However, the fluid flow behavior around the fault damage zone, including where it is supplied and released, remains to be established.

Fluids in the fault damage zone mainly migrate through fractures in the damage zone of the thrust faults. The geometry of fractures is controlled by the tectonic stress and it shows anisotropy. To understand fluid migration around thrust faults, it is essential to know the permeability anisotropy of fractured rock (Saffer and Tobin 2011).

However, the thrust fault that is the seismogenic fault of megathrust earthquakes, such as the Nankai Trough earthquake, is located 5–10 km below the seafloor (Park et al. 2002), which makes in situ permeability measurements difficult. In a previous study, the permeability around the thrust fault was measured by laboratory testing using core specimens or estimated from the wave velocity (e.g., Kato et al. 2004; Nakajima and Uchida 2018). Since the former provided permeability in a shallower area than the seismogenic zone, and the latter provided a low-resolution permeability structure, it is difficult to determine the permeability structure around the thrust fault in the seismogenic zone. In this paper,

the permeability around the thrust fault is determined by estimating paleo-permeability at field scale, which renders high-resolution permeability structure in the seismogenic zone. It is considered that the mineral veins in the outcrop of thrust faults preserve the past hydraulic properties (Otsubo et al. 2020), including permeability. Regarding the permeability, the mineral veins can preserve the past water pathways, thus providing geometric information.

With these objectives in mind, we estimated paleo-permeability from the observable geometric information of the mineral veins in the outcrop based on Oda's permeability tensor theory (Oda 1985). This theory is often used at construction sites, such as underground excavation projects, dams, and geothermal fields, where fluid migration through fractures in the rock mass is problematic (e.g., Oda et al. 1987; Brown and Bruhn 1998; Yamasaki et al. 2015). This tool enables researchers to estimate the permeability tensor from the geometric information of fractures on the surface or borehole wall without measuring the in situ permeability. Ioannou and Spooner (2007) applied Oda's permeability tensor in two dimensions to thermal cracks filled with mineral during the formation of hydrothermal deposits in mining areas. Furthermore, because the quantification of an observed fracture pattern is important in many sub-disciplines of earth sciences, software that can calculate two-dimensional Oda's permeability tensors from image analysis was developed (Healy et al. 2017). However, previous studies centered on this software clearly indicated its limitations, as they were limited to estimating two-dimensional permeability tensor. In contrast, in this study, we have not only applied Oda's permeability tensor theory to estimate three-dimensional paleo-permeability in the damage zone around a thrust fault, but we have also developed in situ analytic methods to estimate a three-dimensional paleo-permeability tensor and identified issues that may affect the general application of these methods to the field. To apply the proposed method, we chose the Nobeoka Thrust fault in Miyazaki Prefecture, southwest Japan. This location is considered to be an onshore analog of the seismogenic fault of the Nankai Trough megathrust earthquake (e.g., Kondo et al. 2005; Okamoto et al. 2008).

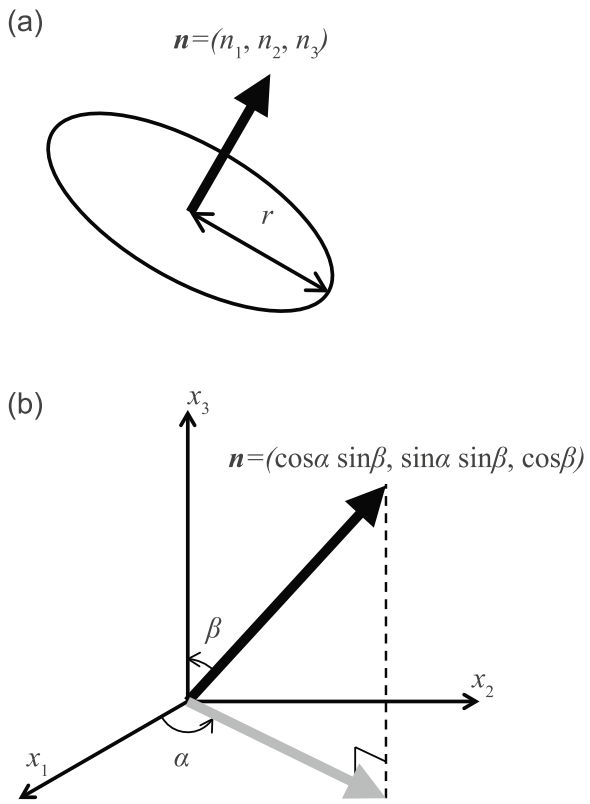

Fig. 1 **a** Geometric definition of the normal unit vector, $\boldsymbol{n}$, of a fracture (or vein) approximated as a disk-shape with a radius, r. **b** Considering the trend as α, and the plunge as β, $\boldsymbol{n}$ can be illustrated as shown in the figure. In this study, x_1, x_2, and x_3 correspond with east, north, and vertical directions (upward being positive), respectively

Methods

Oda's permeability tensor theory

A quartz vein is assumed to be a fracture that once served as a fluid pathway, and its shape is approximated as a disk with two parallel plates in this study. The fracture geometry shown in Fig. 1 was used to calculate the permeability tensor using Oda's permeability tensor (Oda 1985; Oda et al. 2002), where r is the radius of the fracture and $\boldsymbol{n}$ is the normal unit vector of a fracture, which is given by $n_1 = \cos\alpha \sin\beta$, $n_2 = \sin\alpha \sin\beta$, and $n_3 = \cos\beta$, where α is the dip direction and β is the dip angle.

The host rock is assumed to be impermeable when considering the permeability of a fractured rock mass. The water flow along the fracture is assumed such that water movement is idealized to be laminar flow between two parallel plates with an aperture t, and its mean velocity is given by the cubic law. The apparent flow velocity $\bar{v}_i$ (Darcy's velocity) under hydraulic gradient J_j, which is approximated by uniform distribution over a flow domain, is given as (Oda et al. 2002):

$$\bar{v}_i = \frac{\lambda g}{12\nu}\left\{\pi\rho \int_0^{t_m}\int_0^{r_m}\int_{\Omega/2} r^2 t^3\left(\delta_{ij} - n_i n_j\right) \times 2E(\boldsymbol{n}, r, t)\mathrm{d}\Omega\mathrm{d}r\mathrm{d}t\right\}J_j, \tag{1}$$

where λ is the connectivity index (note that $\lambda = 1$ corresponds to the cubic law (e.g., Snow 1969), and the

connectivity index satisfies the inequality $0 \leq \lambda \leq 1$; g is the gravitational acceleration; ν is the kinematic viscosity of water; ρ is the number of fractures per unit volume; δ_{ij} is the Kronecker delta; n_i is the projected length of a unit vector $\boldsymbol{n}$ on the reference axes $x_i (i = 1, 2, 3)$; Ω is the entire solid angle; and $E(\boldsymbol{n}, r, t)$ is a density function that describes the statistical distribution of $\boldsymbol{n}$, r, and t. Here we compare Eq. (1) with Darcy's law, assuming that there is no head loss at the intersection of the fractures, and that λ is determined independently of $\boldsymbol{n}$ and r, such that the permeability tensor k_{ij} can be expressed with the summation convention as follows:

$$k_{ij} = \frac{\lambda}{12}\left(P_{kk}\delta_{ij} - P_{ij}\right), \tag{2}$$

where P_{ij} is a second-rank symmetric tensor that depends only on the geometric aspect of the fractures (Oda 1985) and is given by:

$$P_{ij} = \pi\rho \int_0^{t_m}\int_0^{r_m}\int_{\Omega/2} r^2 t^3 n_i n_j \times 2E(\boldsymbol{n}, r, t)\mathrm{d}\Omega\mathrm{d}r\mathrm{d}t. \tag{3}$$

Determination of P_{ij} from the observable geometric information

The parameters in P_{ij} are related to the fracture (or vein) geometry. However, P_{ij} is not easy to determine because ρ, r, and $\boldsymbol{n}$ are defined in three-dimensional space. The aperture t of the fracture (or vein) can be used to determine P_{ij} in this study, as observed in the two-dimensional section.

If $\boldsymbol{n}$, r, and t in $E(\boldsymbol{n}, r, t)$ are statistically independent, Eq. (3) can be rewritten as follows (note that the method for confirming this assumption is described in detail in the next section):

$$P_{ij} = \pi\rho\langle r^2\rangle\langle t^3\rangle N_{ij}, \tag{4}$$

where:

$$N_{ij} = \int_{\Omega/2} n_i n_j 2E(\boldsymbol{n})\mathrm{d}\Omega, \tag{4a}$$

$$\langle r^2\rangle = \int_0^{r_m} r^2 f(r)\mathrm{d}r, \tag{4b}$$

$$\langle t^3\rangle = \int_0^{t_m} t^3 g(t)\mathrm{d}t, \tag{4c}$$

where N_{ij} is the fabric tensor (Oda 1982, 1984), which is defined using the dip direction α and dip angle β of the mineral veins. Therefore, we can determine N_{ij} from field observations using clinometer measurements. Thus, the fabric tensor represents the stereonet of the strike and dip of a fracture. However, ρ and r are parameters that cannot be determined from the observations. A solution to the problem of determining ρ and r was proposed based on the stereological method (Oda 1985; Oda et al. 2002). Equation (4) can be rewritten as follows:

$$P_{ij} = S_0\langle t^3\rangle N_{ij}, \tag{5}$$

where:

$$S_0 = \pi\rho\langle r^2\rangle = \frac{m(\boldsymbol{q})}{\langle|\boldsymbol{n}\cdot\boldsymbol{q}|\rangle}, \tag{5a}$$

$$\langle|\boldsymbol{n}\cdot\boldsymbol{q}|\rangle = \int_\Omega |\boldsymbol{n}\cdot\boldsymbol{q}|E(\boldsymbol{n})\mathrm{d}\Omega,. \tag{5b}$$

where S_0 is the fracture density ($\mathrm{m}^2/\mathrm{m}^3$) defined by the surface area per unit volume of the analyzed fracture (or vein); $\boldsymbol{q}$ is the unit vector of the scanning line; $m(\boldsymbol{q})$ is the intersection number per unit length; and $\boldsymbol{n}\cdot\boldsymbol{q}$ is the inner product between unit vectors $\boldsymbol{n}$ and $\boldsymbol{q}$.

In summary, the three-dimensional fracture structure P_{ij} can be determined by measuring the aperture t, dip direction α, dip angle β, and intersection number per unit length $m(\boldsymbol{q})$, from the outcrop. When estimating the paleo-permeability, the following assumptions are made in this study with reference to those of Ioannou and Spooner (2007).

1. The host rock is considered impermeable.
2. The measured fracture apertures reflect the original fracture aperture before infilling and the effect of mineral precipitation and dissolution on permeability is not considered (Ioannou and Spooner 2007).
3. All fractures are interconnected (Cox et al. 2001) as all the veins in this study are traces of fluid flow.
4. The cubic law of fluid flow is assumed to hold true. It is known that if the fracture surfaces are in contact or have roughness, the cubic law should be modified using a coefficient, which is determined by fracture surface characteristic factors and/or the fractional contact area and smoothness (e.g., Witherspoon et al. 1980; Zimmerman et al. 1992). However, since the veins in this study are tensile cracks, with a smooth roughness (e.g., Fujii et al. 2007), no contact area, and form an extension stress field with high water pressure, the fracture aperture is considered to approximate that of a parallel plate.

Considering these assumptions, we interpreted the calculated paleo-permeability to have the first order of magnitude at its maximum value. In addition, Oda et al.

(2002) compared experimentally determined and theoretically predicted permeabilities of granite samples with microcracks. Although the permeability tensor in this study is obtained for fractures in mudstone, the results are still valid, as the permeability tensor k_{ij} depends only on the geometry of cracks in the domain. Assuming that pores in the host rock are not the major pathways, the results obtained from this approach are therefore reliable.

Statistical analysis

$E(\boldsymbol{n}, r, t)$ can be written as $E(\boldsymbol{n}), f(r)$, and $g(t)$ when $\boldsymbol{n}$, r, and t are statistically independent. A Chi-square test was conducted for each combination to confirm the independence of the measurements. The dip direction (measured using a clinometer) and the aperture and length of the quartz veins (measured in the field) were used in the Chi-square test. The Chi-square test is a one-tailed test calculated at a significance level of 5%.

The fracture density S_0 is calculated in three dimensions using $m(\boldsymbol{q})$, which can be measured from a two-dimensional cross section using stereology. The scan lines used to calculate S_0 and the number of quartz veins crossing the scan lines $m(\boldsymbol{q})$ must both be statistically homogeneous and represent the elementary volume of a given grid. Therefore, we confirmed the convergence of S_0 by setting the length of the scanning line, which was necessary to determine S_0, as a variable. Furthermore, the Oda's permeability tensor determined by S_0 is the equivalent permeability of a grid that satisfies the representative elementary volume.

Case studies on thrust fault

The permeability tensor was estimated from the geometric information of quartz veins on the outcrop around the Nobeoka Thrust. Here, the estimated permeability tensor refers to the paleo-permeability when the fracture acted as the pathway for fluid migration before the quartz veins formed. The Nobeoka Thrust is a ~ 90-km-long out-of-sequence thrust in Kyushu, Japan. Surface exposures of the Nobeoka Thrust are found in east–west-oriented coastal outcrops in the northeastern part of Nobeoka City, Miyazaki Prefecture, southwest Japan. Murata (1996) reported that the strike and dip of the fault plane is approximately 240°/10°. Recent outcrop surveys and

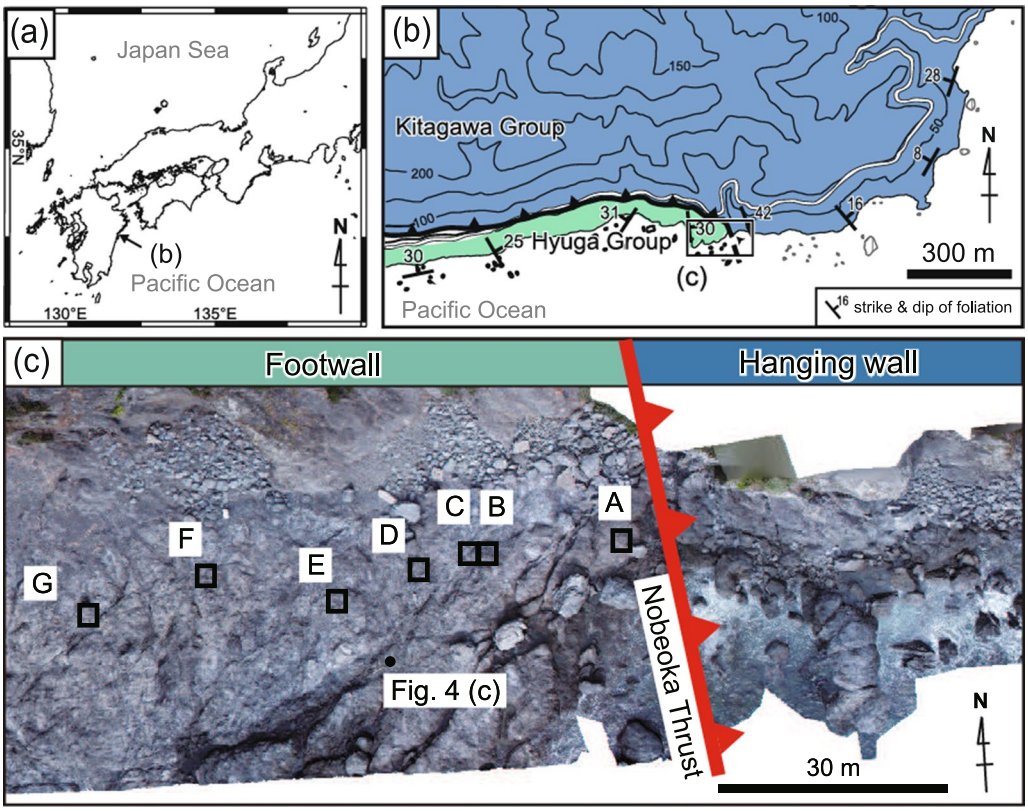

Fig. 2 **a** Location map of the research area. **b** Geological map of study area based on Yamaguchi et al. (2011) and Otsubo et al. (2020). **c** Image of three-dimensional spatial data of the study area. The solid squares indicate grids A–G, and the solid circles indicate the points of quartz vein samples for thin section

borehole investigations in this coastal region have provided a wealth of geological and geophysical data (e.g., Hamahashi et al. 2013; Kimura et al. 2013; Kitajima et al. 2017). In the study area (Fig. 2), the Eocene Kitagawa Group, which is composed of phyllite-dominated terrigenous sediments, including sandstone layers, is exposed in the hanging wall, and the Eocene Hyuga Group, which comprises a shale matrix and a mélange of sandstone and basaltic blocks, is exposed in the footwall (Kondo et al. 2005). Kondo et al. (2005) calculated that the total displacement of the fault plane is 8.6–14.4 km by measuring the vitrinite reflectance (hanging wall, 320 °C; footwall, 250 °C). Mukoyoshi et al. (2009) calculated that the displacement is 6.7–11.6 km by measuring the illite crystallinity (hanging wall, 300 °C; footwall, 250 °C). These were determined considering the assumption that the geothermal gradient is 28–47 °C/km and the dip of the thrust is 10° (Kondo et al. 2005). The stress inversion of the tensile crack-filling vein shows that these fractures were opened by the slip of the Nobeoka Thrust during the earthquake (Otsubo et al. 2016). In addition to these tensile crack-filling veins, the veins observed in the outcrop of the damage zone are classified as fault-filling veins or post-mélange veins (Hamahashi et al. 2015; Kondo et al. 2005; Otsubo et al. 2016; Yamaguchi et al. 2011).

In situ measurements were conducted for the following geometric information of the veins. Of geometric information such as dip direction α, dip angle β, aperture t, and length l were acquired for the quartz veins. Here, t was measured around the middle of the vein observed in the outcrop by placing the crack width ruler, with a lower limit of 0.05 mm (Fig. 3a). Since the veins observed in cross section were protruded by differential erosion, the true aperture could be directly measured for each vein (Fig. 3b). In addition, l was taken as the length of the straight vein that can be observed at the outcrop surface; quartz veins longer than 30 mm, for which strike and dip could be obtained accurately, were measured. For bent veins, they were counted by dividing them into two. Here, the tensile crack-filling vein is considered to have been generated during a single seismic event (Saishu et al. 2017); therefore, the veins with slicken lines on the surface that preserve the shear movement were excluded. Seven grids were then defined to obtain geometric information on quartz veins. Quartz veins that crossed an entire grid were not included, although quartz veins longer than 10 m were observed in coastal outcrops. The outcrop-scale quartz veins were treated as reference values, and thin sections of quartz veins were evaluated along with the type of veins, i.e., whether they were multiple or single, using microscopic observations (Fig. 4).

Seven grids were set up in an east–west direction across the fault [A–G: footwall; Fig. 2c]. The fabric

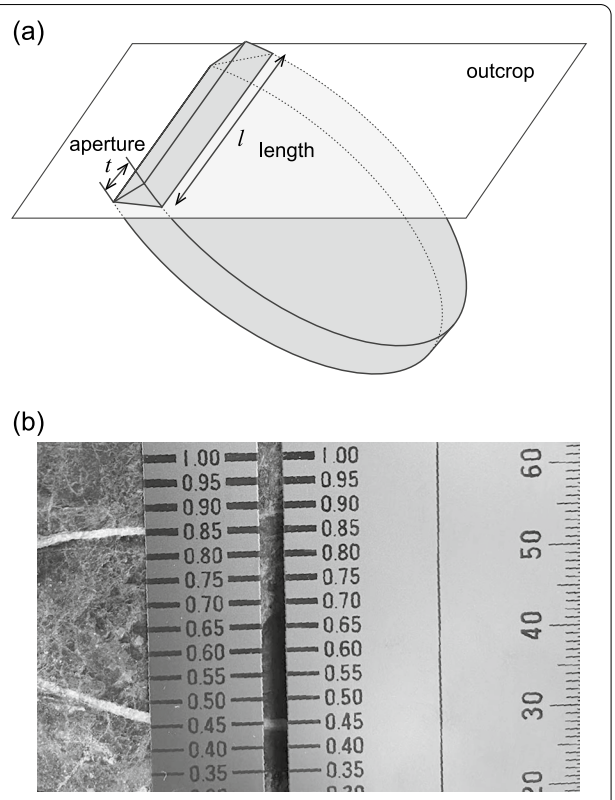

Fig. 3 **a** Schematic illustration of the part of a vein measured in the study. **b** Measurement of the aperture of vein using a crack width ruler. Here, the aperture of vein is 0.85 mm

tensor in a given grid was considered homogeneous if one edge was more than 10 times the average fracture length observed in cross sections within the region (Takemura and Oda 2004, 2005). Therefore, the length of one side of the grid was set as 2.5 m to fully satisfy this condition. Here, the maximum lengths of the veins were measured in advance for all grids, and the roughly estimated average length was used to determine the length of one side of the grid. Furthermore, when setting up the grids, we selected areas without uneven ground to prevent interference with the observation of the veins, and to ensure that these would not be submerged at high tide.

We measured the number of intersections of the scanning line $m(\boldsymbol{q})$ with quartz veins on the trace map to obtain S_0. Here, the quartz vein trace map was drawn using the images of each grid as a base image to measure $m(\boldsymbol{q})$, with both north–south and east–west scanning lines. Furthermore, $m(\boldsymbol{q})$ and $\langle|\boldsymbol{n}\cdot\boldsymbol{q}|\rangle$ were calculated, and the coordinates of the endpoints of the quartz veins on the base trace map were determined using a digitizer. Here, S_0 was estimated using the orientations of both scanning lines. The error due to the placement of the

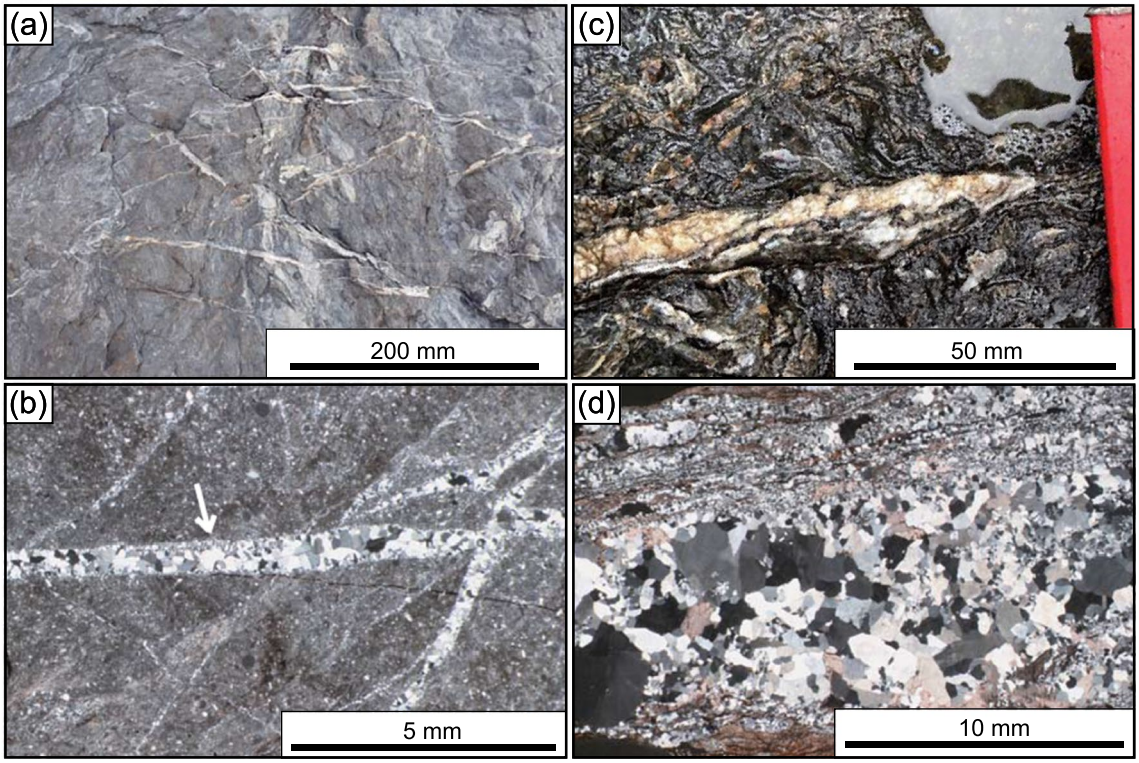

Fig. 4 Photographs of outcrops and photomicrographs of thin sections of quartz veins under crossed Nicol. **a** Shows the quartz veins in the grid F and an arrow in **b** shows the veins near the **a**. Both **a** and **b** formed during a single seismic event. **c**, **d** Show the quartz vein formed during multiple seismic events whose location is indicated as a solid circle in Fig. 2

grid area may be larger than that due to the scanning line because the angles between the scanning line and quartz veins are adjusted by $\langle |\boldsymbol{n} \cdot \boldsymbol{q}| \rangle$ (Oda 1985). The results of the calculations in Takemura and Oda (2004) indicated that the error in the estimated fracture density is within 0.2 if the length of one side of the grid area is at least 10 times the average fracture length.

Results and discussion

Quartz veins in the damage zone

Photographs of outcrops and photomicrographs of thin sections of typical quartz veins that were observed are shown in Fig. 4. Figure 4a, b indicates no evidence of repeated fracture sealing because the quartz grains grew only on the vein surface, with no confirmation of an inclusion band in the quartz veins. In contrast, Fig. 4c, d shows repeated sealing in the quartz veins based on the evolution of quartz growth in the fractures. This is consistent with the results of Saishu et al. (2017), where it was found that quartz veins most likely formed due to a single seismic event, as the tensile cracks opened in response to an event and did not reopen after they were filled by quartz. Therefore, the quartz veins were used for measurement in this study because they were most likely formed during a single event.

Stereonet projections of the analyzed quartz veins are shown in Fig. 5. Grids A, B–D, and E–G exhibit E–W, NNE–SSW, and N–S quartz vein orientations, respectively. Bimodal poles were observed for the quartz veins in grids A (223°/44° and 150°/53°), B (120°/15° and 254°/46°), and D (205°/41° and 304°/27°). Unimodal poles were observed for quartz veins in the C (304°/15°), E (284°/7°), F (270°/3°), and G (106°/7°) grids.

Statistical features and parameters

Parameters N_{ij}, t and S_0 are required to estimate the three-dimensional permeability tensor. Among these three parameters, N_{ij} calculated based on α and β, and t, are the most reliable because they are measured directly. When α and β is measured with a clinometer on an outcrop, mineral veins parallel to the plane are generally difficult to observe. However, as the study area is a coastal outcrop with an uneven ground, quartz veins with a near-horizontal dip have been well measured. Furthermore, the statistical independence of $\boldsymbol{n}$ and r, t for $E(\boldsymbol{n}, r, t)$ in Eq. (5) is required.

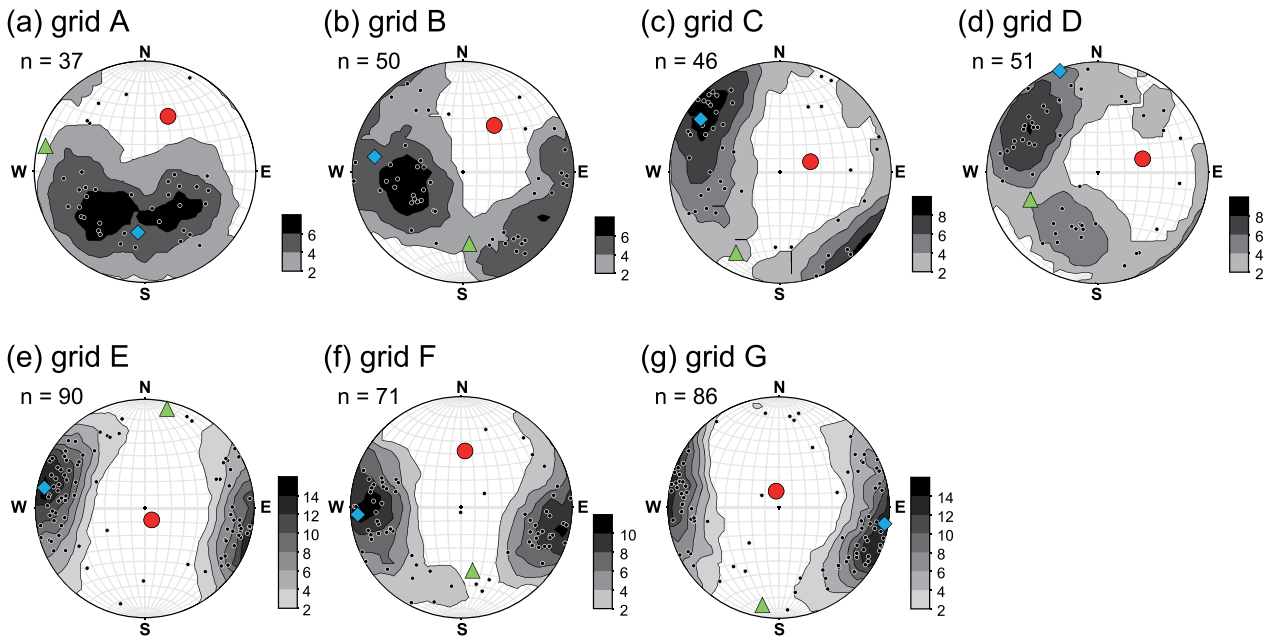

Fig. 5 Dots indicate poles of the tensile crack-filling veins in the damage zone of Nobeoka Thrust. The contour in stereonet was based on the Kamb contouring method with contour interval 2.0. The maximum, intermediate, and minimum permeability directions are indicated by circles, triangles, and diamonds, respectively. All plots are on the lower hemisphere of the Wulff net

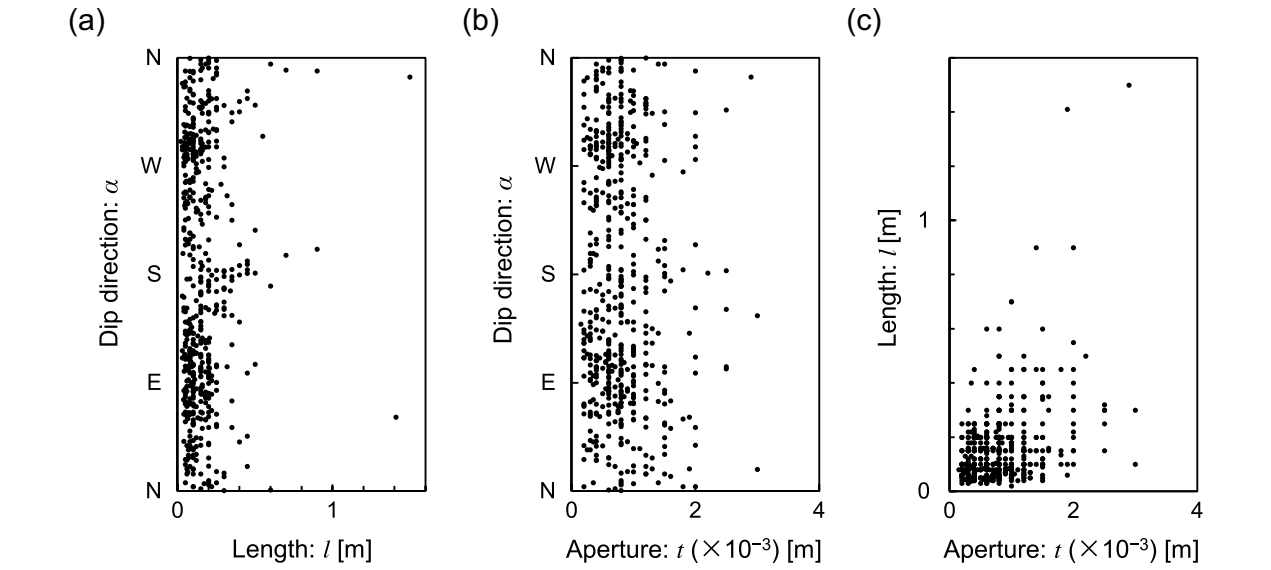

Fig. 6 Data for quartz veins with Chi-square test as statistical analysis. **a** Relationship between dip directions and length of veins. **b** Relationship between dip directions and aperture of veins. **c** The horizontal axis of the graph is apertures and the vertical axis is lengths of veins

The relationships between the dip direction, length, and aperture are shown in Fig. 6. The Chi-square test results for dip direction-length, dip direction-aperture, and length and aperture of the observed quartz veins are $P = 1.35 \times 10^{-3}$ %, $P = 2.10$ %, and $P = 9.90 \times 10^{-7}$ %, respectively, where P is the probability value. All relationships were below $P = 5$ %, and the statistical hypothesis was rejected when the significance level of the one-tailed test was set at 5%. These results indicate that the direction, length, direction, and aperture were statistically independent of each other. Here, the low probability value between the aperture and length may

be because of the different aspect ratios in the three dimensions ($t/2r$) or those in the two dimensions (t/l) for each quartz vein.

The surface area of the quartz veins in a unit volume, S_0, was estimated based on stereology in this study. The $m(\boldsymbol{q})$ used in the calculation of S_0 depends on the length of the scanning line. To reduce this deviation, the scanning lines should be sufficiently long. Figure 7 shows photographs and trace maps of the quartz veins of the seven grids. S_0 was calculated from these trace maps, and the dependence of S_0 on the total scanning line lengths, from 2.5 to 40 m, is shown in Fig. 7. Here, the vertical axis shows the relative error, $\mathrm{R.E} = \left|1 - \left(m(\boldsymbol{q})/m(\boldsymbol{q})_{\mathrm{Ave.}}\right)\right|$, where $m(\boldsymbol{q})_{\mathrm{Ave.}}$ is the average value of $m(\boldsymbol{q})$ for each grid, which is used to evaluate the scanning line length required for convergence (e.g., Kanit et al. 2003). As shown in Fig. 8, S_0 begins to converge at a scanning line length of ~ 20 m for the entire grid. In this study, the total scanning line length was set to 30 m, which falls within the relative error of 0.2 (20%). Fracture density S_0 is estimated from the number of veins intersecting the scanning line, as measured on the two-dimensional plane, $m(\boldsymbol{q})$. Therefore, the error in the estimated paleo-permeability in this study was within 20%.

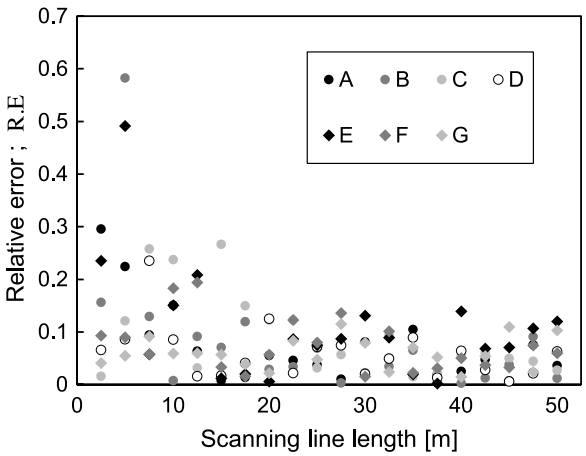

Fig. 8 Variation of the surface area per unit volume of fractures (or veins), S_0, in each grid with the total lengths of the scanning lines

Estimated paleo-permeability tensor

The estimated paleo-permeability and related parameters are shown in Table 1 and Fig. 9. The average length l of the quartz veins in each grid was 0.09–0.22 m. The average aperture t of the quartz veins in each grid was $0.62–1.27 \times 10^{-3}$ m. The average fracture density S_0 of

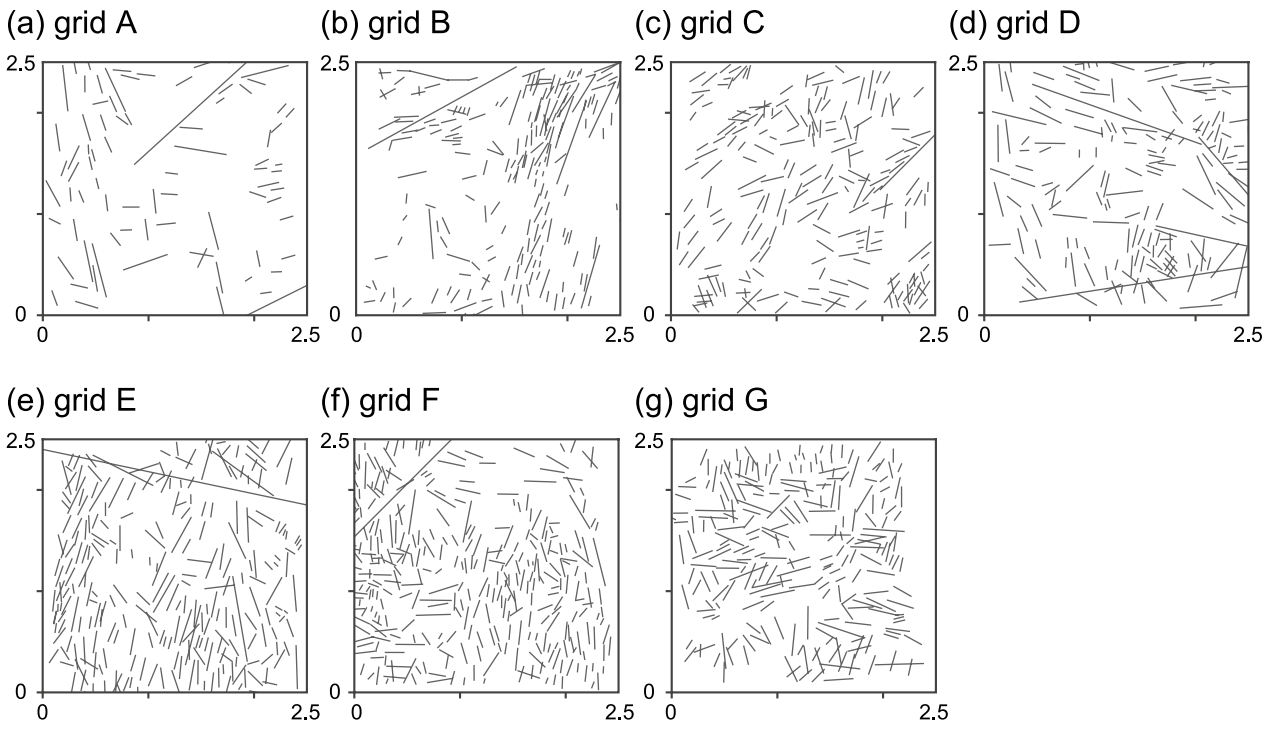

Fig. 7 **a**–**g** Trace maps of veins in grids A to G. The sides of each grid are approximately 2.5 m long. Horizontal and vertical axes represent easting and northing, respectively

Table 1 List of measurement data, surface area per unit volume of mineral veins, and paleo-permeability tensor

Grid	l [m]	t ($\times 10^{-3}$) [m]	S_0 [m^2/m^3]	k_{ij} [m^2]	k_i [m^2]
A	0.22	1.27	4.01	$\begin{pmatrix} 1.12\times10^{-9} & 5.71\times10^{-12} & -6.87\times10^{-11} \\ & 9.33\times10^{-10} & -3.46\times10^{-10} \\ sym. & & 9.62\times10^{-10} \end{pmatrix}$	$\begin{pmatrix} 1.31\times10^{-9} \\ 1.11\times10^{-9} \\ 5.98\times10^{-10} \end{pmatrix}$
B	0.11	0.85	7.43	$\begin{pmatrix} 3.61\times10^{-10} & 3.78\times10^{-11} & -5.68\times10^{-11} \\ & 4.31\times10^{-10} & -5.67\times10^{-11} \\ sym. & & 4.61\times10^{-10} \end{pmatrix}$	$\begin{pmatrix} 5.32\times10^{-10} \\ 3.88\times10^{-10} \\ 3.34\times10^{-10} \end{pmatrix}$
C	0.11	0.73	6.39	$\begin{pmatrix} 2.22\times10^{-10} & 4.84\times10^{-11} & -4.84\times10^{-11} \\ & 2.49\times10^{-10} & 4.44\times10^{-12} \\ sym. & & 3.37\times10^{-10} \end{pmatrix}$	$\begin{pmatrix} 3.56\times10^{-10} \\ 2.77\times10^{-10} \\ 1.74\times10^{-10} \end{pmatrix}$
D	0.12	0.81	9.40	$\begin{pmatrix} 8.48\times10^{-10} & 4.96\times10^{-11} & -1.36\times10^{-10} \\ & 7.16\times10^{-10} & -3.92\times10^{-11} \\ sym. & & 9.67\times10^{-10} \end{pmatrix}$	$\begin{pmatrix} 1.07\times10^{-9} \\ 7.66\times10^{-10} \\ 6.99\times10^{-10} \end{pmatrix}$
E	0.14	0.67	11.96	$\begin{pmatrix} 2.97\times10^{-10} & 8.57\times10^{-11} & -5.92\times10^{-11} \\ & 6.99\times10^{-10} & 2.37\times10^{-11} \\ sym. & & 7.96\times10^{-10} \end{pmatrix}$	$\begin{pmatrix} 8.05\times10^{-10} \\ 7.15\times10^{-10} \\ 2.72\times10^{-10} \end{pmatrix}$
F	0.09	0.71	11.14	$\begin{pmatrix} 2.52\times10^{-10} & -1.57\times10^{-11} & -3.59\times10^{-11} \\ & 5.60\times10^{-10} & -4.65\times10^{-11} \\ sym. & & 5.65\times10^{-10} \end{pmatrix}$	$\begin{pmatrix} 6.09\times10^{-10} \\ 5.20\times10^{-10} \\ 2.47\times10^{-10} \end{pmatrix}$
G	0.14	0.62	10.21	$\begin{pmatrix} 1.20\times10^{-10} & 1.90\times10^{-11} & 9.89\times10^{-12} \\ & 2.46\times10^{-10} & -1.19\times10^{-11} \\ sym. & & 2.96\times10^{-10} \end{pmatrix}$	$\begin{pmatrix} 2.99\times10^{-10} \\ 2.47\times10^{-10} \\ 1.16\times10^{-10} \end{pmatrix}$

Here, k_i is the principal permeability of k_{ij}

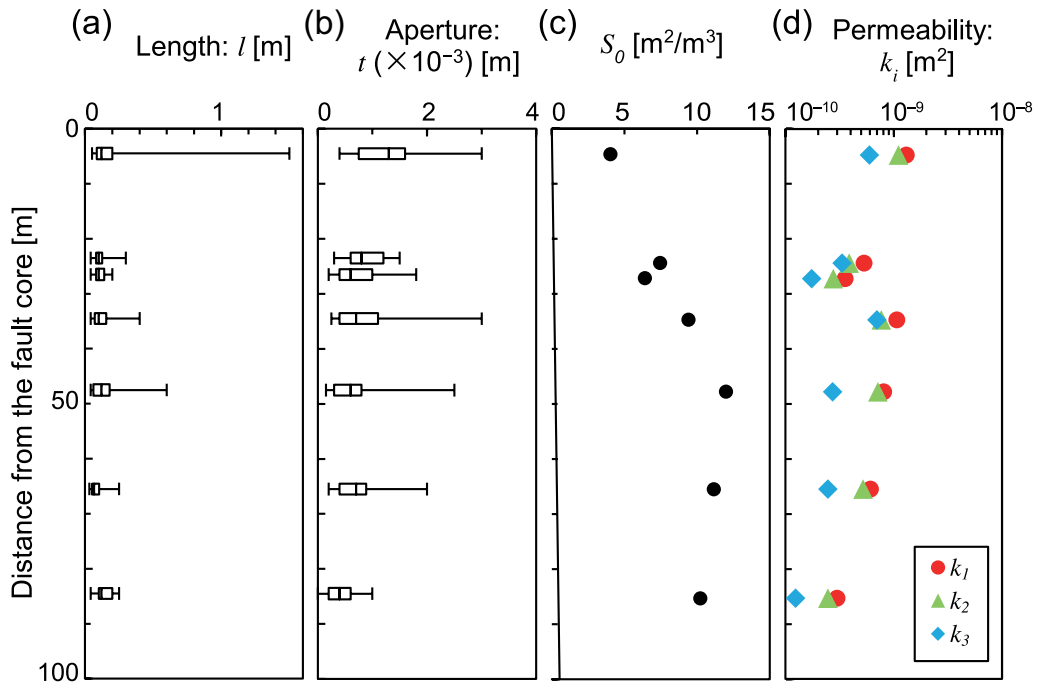

Fig. 9 Summary of measurement data, and result of estimation. The variation of the **a** length l, **b** aperture t, **c** S_0, and **d** paleo-permeability k_i with the distance from the fault core

the quartz veins in each grid was 4.01–11.96 m^2/m^3. The maximum permeability k_1 was 2.99×10^{-10} to 1.31×10^{-9} m^2, the intermediate permeability k_2 was 2.47×10^{-10} to 1.11×10^{-9} m^2, and the minimum permeability k_3 was 1.16×10^{-10} to 6.99×10^{-10} m^2. Here, k_i is the principal permeability of k_{ij}.

In the current Nankai Trough subduction zone, laboratory experiments using drilling cores shallower than 500 m below the seafloor have permeabilities of 10^{-20} to 10^{-15} m^2 (Ikari et al. 2009; Tanikawa et al. 2012; Tanikawa et al. 2014). These permeabilities were measured from core size specimens and were smaller than the permeability at the field scale. This is because wider and longer open fractures are not reflected in core size permeability. Comparing the field-scale paleo-permeability of previous studies, 10^{-10}–10^{-5} m^2 was determined for thermal fluid (Ioannou and Spooner 2007) and 10^{-14}–10^{-9} m^2 for oceanic crust (Gilbert et al. 2018) based on mineral vein widths and densities. Gilbert et al. (2018) estimated the permeability from the width and density of mineral veins and did not separate them by direction. In this case, the permeability without considering the anisotropy is represented by the average value, $k_{ii}/3 (= (k_{11} + k_{22} + k_{33})/3)$, of the permeability tensor, k_{ij}, and should be slightly underestimated compared to the maximum principal permeability, k_1. Therefore, if the anisotropy of the principal permeability is discussed, the permeability is suitable to be represented in the form of a tensor.

Paleo-permeability in the damage zone

The estimated maximum paleo-permeability, k_1, which is approximately perpendicular to the fault plane, suggests that the fluid migrated more readily toward the fault plane or hanging wall. The relationship between the maximum, intermediate, and minimum paleo-permeabilities and the angle of the veins can be classified into three categories, as follows. Grids E and F exhibit a $k_1 \approx k_2 > k_3$ relationship, and the angle of the analyzed quartz veins is mostly constant, suggesting the development of a single system. Grids A, C, and G exhibited a $k_1 > k_2 > k_3$ relationship, with a high degree of variability among the quartz veins and the development of a single system. Here, the vein in Grid A had a low permeability despite its longer fracture and thicker aperture. This may be because the veins in Grid A had more horizontally oriented veins than other Grids; therefore, the S_0 may have been underestimated. Grids B and D exhibited a $k_1 > k_2 \approx k_3$ relationship. When k_2 and k_3 are approximately the same and k_1 is dominant, the poles of veins have a bimodal tendency. These results indicate that the flow direction of the intermediate paleo-permeability, k_2, depends on the variability of the fracture orientation.

The change in the paleo-permeability of the footwall with the distance from the fault core was studied. The paleo-permeability of grid A, which is the closest grid to the fault core, was high, with the highest paleo-permeability observed in the footwall. Paleo-permeability near a given fault is often studied because it is directly related to subsurface mass transport, and paleo-permeability in the damage zone increases as the fault core approaches (e.g., Evans et al. 1997; Lockner et al. 2009). Our results correspond with those of Lockner et al. (2009), who noted that permeability was particularly high in the damage zone, ~ 10 m from the fault core. Many quartz veins with wide apertures were observed in Grid A. Therefore, we show that the paleo-permeability is higher in Grid A because it is affected by the cube of the fracture aperture.

Concluding remarks

The purpose of this study was to estimate three-dimensional paleo-permeability based on the geometric information of mineral veins observed in an outcrop of a damage zone around a thrust fault. Additionally, in situ data analytical techniques were developed to estimate the three-dimensional paleo-permeability tensor based on Oda's permeability tensor theory. Furthermore, we estimated the paleo-permeability around the Nobeoka Thrust based on geometric patterns of exposed mineral veins. The conclusions are summarized as follows:

(1) The three-dimensional permeability can be estimated using stereology, considering the statistical independence of the aperture, length, and orientation, and the scanning line length required for a representative elementary volume. We estimated the maximum, intermediate, and minimum permeabilities and the associated direction of flow in three dimensions.
(2) The required scanning line length for determining S_0 is 30 m. The r, l, and $\boldsymbol{n}$ values of the quartz veins in the study area are statistically independent of each other. Therefore, the proposed method, which analyzes observable geometric information, is a viable approach for three-dimensional permeability estimation. However, it is necessary to confirm the method for analyzing anisotropic veins and/or the relationship between vein density and connectivity through numerical calculations in future work.
(3) The estimated three-dimensional paleo-permeability shows that the fluid in the footwall tends to migrate toward the fault plane or to the hanging wall. This result is consistent with the fault-valve model because they suggest that the accumulated

fluid pressure along the fault plane before an earthquake dissipates to the fault plane or hanging wall immediately after the earthquake.

Acknowledgements
We thank honorary professor M. Oda from Saitama University for the useful discussions about permeability tensor. We express our sincere thanks to the reviewers and Associate Editor for reading the manuscript and giving us many important comments. This work was supported by Sasakawa Scientific Research Grant 2021-2029 from The Japan Science Society and JSPS KAKENHI Grant Number 19K04603 and 19K04046.

Author contributions
HH carried out the numerical analysis and drafted the manuscript. TT proposed the topic, conceived, and drafted the manuscript of theoretical part. MO and DA contributed to the discussion of the results. All authors read and approved the final manuscript.

Funding
This work was supported by Sasakawa Scientific Research Grant 2021-2029 from The Japan Science Society and JSPS KAKENHI Grant Number 19K04603 and 19K04046.

Availability of data and materials
Not applicable.

Declarations

Consent for publication
Not applicable.

Competing interests
The authors declare that they have no competing interests.

Author details
[1]Geomechanics Lab., Graduate School of Integrated Basic Sciences, Nihon University, Sakurajyosui 3-25-40, Setagaya, Tokyo 156-8550, Japan. [2]Geological Survey of Japan, Research Institute of Earthquake and Volcano Geology, AIST, Tsukuba Central 7, 1-1-1 Higashi, Tsukuba 305-8567, Japan.

Received: 9 April 2022 Accepted: 22 August 2022
Published online: 19 September 2022

References

Bangs NL (1990) Seismic velocities from the Barbados ridge complex: indicators of high pore fluid pressures in an accretionary complex. J Geophys Res 95:8767–8782. https://doi.org/10.1029/JB095iB06p08767

Brown SR, Bruhn RL (1998) Fluid permeability of deformable fracture networks. J Geophys Res Solid Earth 103(2):2489–2500. https://doi.org/10.1029/97jb03113

Cox SF, Knackstedt MA, Braun J (2001) Principles of structural control on permeability and fluid flow in hydrothermal systems. In: Richards JP, Tosdal RM (eds) Reviews in economic geology: structural controls on ore genesis. vol 14. Society of Economic Geologists, pp. 1–24. https://doi.org/10.5382/Rev.14.01

Evans JP, Forster CB, Goddard JV (1997) Permeability of fault-related rocks, and implications for hydraulic structure of fault zones. J Struct Geol 19(11):1393–1404. https://doi.org/10.1016/S0191-8141(97)00057-6

Fujii Y, Takemura T, Takahashi M, Lin W (2007) Surface features of uniaxial tensile fractures and their relation to rock anisotropy in Inada granite. Int J Rock Mech Min Sci 44(1):98–107. https://doi.org/10.1016/j.ijrmms.2006.05.001

Gilbert LA, Crispini L, Tartarotti P, Bona ML (2018) Permeability structure of the lava-dike transition of 15-Myr-old oceanic crust formed at the East Pacific Rise. Geochem Geophys Geosyst 19(9):3555–3569. https://doi.org/10.1029/2018gc007696

Hamahashi M, Saito S, Kimura G, Yamaguchi A, Fukuchi R, Kameda J, Hamada Y, Kitamura Y, Fujimoto K, Hashimoto Y, Hina S, Eida M (2013) Contrasts in physical properties between the hanging wall and footwall of an exhumed seismogenic megasplay fault in a subduction zone-An example from the Nobeoka Thrust Drilling Project. Geochem Geophys Geosyst 14(12):5354–5370. https://doi.org/10.1002/2013gc004818

Hamahashi M, Hamada Y, Yamaguchi A, Kimura G, Fukuchi R, Saito S, Kameda J, Kitamura Y, Fujimoto K, Hashimoto Y (2015) Multiple damage zone structure of an exhumed seismogenic megasplay fault in a subduction zone—a study from the Nobeoka Thrust Drilling Project. Earth Planets Space 67(1):30. https://doi.org/10.1186/s40623-015-0186-2

Healy D, Rizzo RE, Cornwell DG, Farrell NJC, Watkins H, Timms NE, Gomez-Rivas E, Smith M (2017) FracPaQ: a MATLAB™ toolbox for the quantification of fracture patterns. J Struct Geol 95:1–16. https://doi.org/10.1016/j.jsg.2016.12.003

Hubbert MK, Rubey WW (1959) Role of fluid pressure in mechanics of overthrust faulting: I. Mechanics of fluid-filled porous solids and its application to overthrust faulting. Bull Geol Soc Am 70(2):115–166. https://doi.org/10.1130/0016-7606(1959)70[115:ROFPIM]2.0.CO;2

Ikari MJ, Saffer DM, Marone C (2009) Frictional and hydrologic properties of clay-rich fault gouge. J Geophys Res 114 (B5). https://doi.org/10.1029/2008jb006089

Ioannou SE, Spooner ETC (2007) Fracture analysis of a volcanogenic massive sulfide-related hydrothermal cracking zone, Upper Bell River Complex, Matagami, Quebec: application of permeability tensor theory. Econ Geol 102(4):667–690. https://doi.org/10.2113/gsecongeo.102.4.667

Kamei R, Pratt RG, Tsuji T (2012) Waveform tomography imaging of a megasplay fault system in the seismogenic Nankai subduction zone. Earth Planet Sci Lett 317–318:343–353. https://doi.org/10.1016/j.epsl.2011.10.042

Kanit T, Forest S, Galliet I, Mounoury V, Jeulin D (2003) Determination of the size of the representative volume element for random composites: statistical and numerical approach. Int J Solids Struct 40(13):3647–3679. https://doi.org/10.1016/S0020-7683(03)00143-4

Kato A, Sakaguchi A, Yoshida S, Yamaguchi H, Kaneda Y (2004) Permeability structure around an ancient exhumed subduction-zone fault. Geophys Res Lett 31 (6). https://doi.org/10.1029/2003GL019183

Kimura G, Hamahashi M, Sy O, Yamaguchi A, Kameda J, Raimbourg H, Hamada Y, Yamaguchi H, Shibata T (2013) Hanging wall deformation of a seismogenic megasplay fault in an accretionary prism: the Nobeoka Thrust in southwestern Japan. J Struct Geol 52:136–147. https://doi.org/10.1016/j.jsg.2013.03.015

Kitajima H, Takahashi M, Otsubo M, Saffer D, Kimura G (2017) Strength and deformation behavior of the Shimanto accretionary complex across the Nobeoka thrust. Island Arc 26(4):e12192. https://doi.org/10.1111/iar.12192

Kondo H, Kimura G, Masago H, Ohmori-Ikehara K, Kitamura Y, Ikesawa E, Sakaguchi A, Yamaguchi A, Okamoto Sy (2005) Deformation and fluid flow of a major out-of-sequence thrust located at seismogenic depth in an accretionary complex: Nobeoka Thrust in the Shimanto Belt, Kyushu, Japan. Tectonics 24 (6). https://doi.org/10.1029/2004tc001655

Lockner DA, Tanaka H, Ito H, Ikeda R, Omura K, Naka H (2009) Geometry of the Nojima Fault at Nojima-Hirabayashi, Japan—I. A simple damage structure inferred from borehole core permeability. Pure Appl Geophys 166(10):1649–1667. https://doi.org/10.1007/s00024-009-0515-0

Mukoyoshi H, Hirono T, Hara H, Sekine K, Tsuchiya N, Sakaguchi A, Soh W (2009) Style of fluid flow and deformation in and around an ancient out-of-sequence thrust: an example from the Nobeoka Tectonic Line in the Shimanto accretionary complex, Southwest Japan. Island Arc 18(2):333–351. https://doi.org/10.1111/j.1440-1738.2009.00670.x

Murata A (1996) Nappe structures of the Shimanto terrane of the Mikado-Osuzuyama area in East Kyushu. Nat Sci Res Faculty Integr Arts Sci Univ Tokushima 9:49–61

Nakajima J, Uchida N (2018) Repeated drainage from megathrusts during episodic slow slip. Nat Geosci 11(5):351–356. https://doi.org/10.1038/s41561-018-0090-z

Oda M (1982) Fabric tensor for discontinuous geological materials. Soils Found 22(4):96–108. https://doi.org/10.3208/sandf1972.22.4_96

Oda M (1984) Similarity rule of crack geometry in statistically homogeneous rock masses. Mech Mater 3(2):119–129. https://doi.org/10.1016/0167-6636(84)90003-6

Oda M (1985) Permeability tensor for discontinuous rock masses. Géotechnique 35(4):483–495. https://doi.org/10.1680/geot.1985.35.4.483
Oda M, Hatsuyama Y, Ohnishi Y (1987) Numerical experiments on permeability tensor and its application to jointed granite at Stripa Mine, Sweden. J Geophys Res 92(B8):8037–8037. https://doi.org/10.1029/JB092iB08p08037
Oda M, Takemura T, Aoki T (2002) Damage growth and permeability change in triaxial compression tests of Inada granite. Mech Mater 34(6):313–331. https://doi.org/10.1016/S0167-6636(02)00115-1
Okamoto A, Kikuchi T, Tsuchiya N (2008) Mineral distribution within polymineralic veins in the Sanbagawa belt, Japan: implications for mass transfer during vein formation. Contrib Miner Petrol 156(3):323–336. https://doi.org/10.1007/s00410-008-0288-y
Otsubo M, Miyakawa A, Kawasaki R, Sato K, Yamaguchi A, Kimura G (2016) Variations in stress and driving pore fluid pressure ratio using vein orientations along megasplay faults: example from the Nobeoka Thrust, Southwest Japan. Island Arc 25(6):421–432. https://doi.org/10.1111/iar.12155
Otsubo M, Hardebeck JL, Miyakawa A, Yamaguchi A, Kimura G (2020) Localized fluid discharge by tensile cracking during the post-seismic period in subduction zones. Sci Rep 10(1):12281. https://doi.org/10.1038/s41598-020-68418-z
Park J-O, Tsuru T, Kodaira S, Cummins Phil R, Kaneda Y (2002) Splay fault branching along the Nankai subduction zone. Science 297(5584):1157–1160. https://doi.org/10.1126/science.1074111
Park J-O, Fujie G, Wijerathne L, Hori T, Kodaira S, Fukao Y, Moore GF, Bangs NL, Si K, Taira A (2010) A low-velocity zone with weak reflectivity along the Nankai subduction zone. Geology 38(3):283–286. https://doi.org/10.1130/g30205.1
Saffer DM, Tobin HJ (2011) Hydrogeology and mechanics of subduction zone forearcs: fluid flow and pore pressure. Annu Rev Earth Planet Sci 39(1):157–186. https://doi.org/10.1146/annurev-earth-040610-133408
Saishu H, Okamoto A, Otsubo M (2017) Silica precipitation potentially controls earthquake recurrence in seismogenic zones. Sci Rep 7(1):13337. https://doi.org/10.1038/s41598-017-13597-5
Scholz CH (2019) The mechanics of earthquakes and faulting. 3 edn. Cambridge University Press, Cambridge. https://doi.org/10.1017/9781316681473
Sibson RH (1981) Fluid flow accompanying faulting: field evidence and models. In: Simpson DW, Richards PG (eds) Earthquake prediction: an international review. vol Maurice Ewing Series. AGU, pp 593–603. https://doi.org/10.1029/ME004p0593
Sibson RH (1990) Conditions for fault-valve behaviour. Geol Soc London Spl Publ 54(1):15. https://doi.org/10.1144/GSL.SP.1990.054.01.02
Sibson RH (1992) Implications of fault-valve behaviour for rupture nucleation and recurrence. Tectonophysics 211(1):283–293. https://doi.org/10.1016/0040-1951(92)90065-E
Sibson RH (2020) Preparation zones for large crustal earthquakes consequent on fault-valve action. Earth Planets Space 72 (1). https://doi.org/10.1186/s40623-020-01153-x
Snow DT (1969) Anisotropie permeability of fractured media. Water Resour Res 5(6):1273–1289. https://doi.org/10.1029/WR005i006p01273
Takemura T, Oda M (2005) Changes in crack density and wave velocity in association with crack growth in triaxial tests of Inada granite. J Geophys Res. 110 (B5). https://doi.org/10.1029/2004jb003395.
Takemura T, Oda M (2004) Stereology-based fabric analysis of microcracks in damaged granite. Tectonophysics 387(1–4):131–150. https://doi.org/10.1016/j.tecto.2004.06.004
Tanikawa W, Mukoyoshi H, Lin W, Hirose T, Tsutsumi A (2014) Pressure dependence of fluid transport properties of shallow fault systems in the Nankai subduction zone. Earth Planets Space 66(1):90. https://doi.org/10.1186/1880-5981-66-90
Tanikawa W, Mukoyoshi H, Tadai O, Hirose T, Tsutsumi A, Lin W (2012) Velocity dependence of shear-induced permeability associated with frictional behavior in fault zones of the Nankai subduction zone. J Geophys Res Solid Earth 117 (B5). https://doi.org/10.1029/2011JB008956.
Tsuji T, Ashi J, Ikeda Y (2014) Strike-slip motion of a mega-splay fault system in the Nankai oblique subduction zone. Earth Planets Space 66(1):120. https://doi.org/10.1186/1880-5981-66-120
Witherspoon PA, Wang JSY, Iwai K, Gale JE (1980) Validity of cubic law for fluid flow in a deformable rock fracture. Water Resour Res 16(6):1016–1024. https://doi.org/10.1029/WR016i006p01016
Yamaguchi A, Cox SF, Kimura G, Sy O (2011) Dynamic changes in fluid redox state associated with episodic fault rupture along a megasplay fault in a subduction zone. Earth Planet Sci Lett 302(3):369–377. https://doi.org/10.1016/j.epsl.2010.12.029
Yamasaki M, Ttusaka K, Otani T, Shinji M (2015) Permeability estimation based on crack tensor on site scale. J Jap Soc Civil Eng Ser F2 Undergr Space Res. 71(1):1–10. https://doi.org/10.2208/jscejusr.71.1
Zimmerman RW, Chen D-W, Cook NGW (1992) The effect of contact area on the permeability of fractures. J Hydrol 139(1):79–96. https://doi.org/10.1016/0022-1694(92)90196-3

Publisher's Note